Eur. Phys. J. Appl. Phys. (2014) 68: 10101
DOI: 10.1051/epjap/2014140060

THE EUROPEAN PHYSICAL JOURNAL
APPLIED PHYSICS

Review Article

Atom probe tomography in nanoelectronics

Didier Blavette[a] and Sébastien Duguay

Normandie University, Groupe de Physique des Matériaux, UMR CNRS 6634, ESP CARNOT Institute, 76800 St. Etienne du Rouvray Cedex, France

Received: 12 February 2014 / Received in final form: 16 July 2014 / Accepted: 24 July 2014
Published online: 26 September 2014 – © EDP Sciences 2014

Abstract. The role of laser assisted atom probe tomography (APT) in microelectronics is discussed on the basis of various illustrations related to SiGe epitaxial layers, bipolar transistors or MOS nano-devices including gate all around (GAA) devices that were carried out at the Groupe de Physique des Matériaux of Rouen (France). 3D maps as provided by APT reveal the atomic-scale distribution of dopants and nanostructural features that are vital for nanoelectronics. Because of trajectory aberrations, APT images are subjected to distortions and local composition at the nm scale may either be biased. Procedures accounting for these effects were applied so that to correct images.

1 Introduction

Microelectronics has been the witness of considerable progresses in terms of miniaturisation of ultra large scale integrated circuits. The latest technological node of Intel MOS-FET nanotransistors is for instance 22 nm, a scale that poses new challenges. Such low dimensions requires for instance ultra-shallow junctions that need to be heavily doped to maintain good conductance of the channel between source and drain of MOS-FET transistors. However such high dopant levels may exceed the solubility limit in the semiconductor (Si, Ge...) leading consequently to clustering or precipitation of dopants that consequently reduce their electrical activity. In this context, atom probe tomography (APT) is appealed to play an increasing role. APT is able to map out at the ultimate scale the spatial distribution of chemical species within a small volume (~100 nm^3).

Secondary ion mass spectrometry (SIMS) has been the reference tool in microelectronics for dopant profiling in semiconductors. However, SIMS faces its ultimate limits for latest generation transistors and this technique is unable to image dopant segregation at the desired scale (nm) and in 3D. Because of its high spatial resolution (0.1 nm in depth and a few tenths of a nm at the sample surface) and 3D imaging capability, laser-assisted APT is called to play an increasing role in microelectronics.

Segregation of P or As to lattice defects (grain boundaries) has been shown for instance to occur using APT [1]. Distribution of boron or Pt in NiSi silicides used in contacts of transistors [2,3], clustering of boron in heavily implanted silicon [4,5], Cottrell atmospheres in arsenic-implanted silicon [6] were recently investigated demonstrating the nearly atomic-scale resolution and quantitativity of APT for semi-conductors [7,8]. Besides, the characteristic size of latest generation nanotransistors, that is basically two times a technological node (~50 nm) is now below the APT field of view (~100 × 100 nm^2) so that 3D reconstruction of the distribution of the device and of dopants is now achievable. FIB (focused ion beam) milling and lift-out techniques have played here a major role in the preparation of samples in the suitable form of sharply pointed needles [9].

With the increase of miniaturisation the Moore's law faces new physical limits and new challenges emerge. In addition to the ultimate scale to which nano-devices need to be investigated, new generations of integrated circuits are architectured in the three dimensions of spaces (ex: FinFETs) and hence require 3D microscopy and microanalysis. In this context, again SIMS faces to its ultimate limits. APT is now appeal to play a key role in the development of tomorrow nanodevices [6]. Number of manufacturers among them IBM, Intel, Samsung or Toshiba already use this instrument for the design of last generation devices.

In this article, the role of APT in microelectronics is illustrated through recent investigations dealing with (SiGe, SiAs) epitaxial layers, bipolar transistors as well as MOS devices and gate all around (GAA) transistors. Local magnification effects due to ion trajectory aberrations, and related composition bias as well as image distortion effects are discussed. Some possible routes to correct such affects in APT reconstructions are presented.

2 Atom probe tomography

Atom probe tomography (APT) is an extension in 3D of the atom-probe field ion microscope (APFIM), an

[a] e-mail: didier.blavette@univ-rouen.fr

https://doi.org/10.1051/epjap/2014140060 Published online by Cambridge University Press

instrument designed in the late 1960s by Müller and coworkers [10]. APT is the only approach able to map out the 3D distribution of chemical species in a material at the atomic-scale. The principle of APT is based on the field evaporation of surface atoms of the specimen (a sharply pointed needle, $R \sim 50$ nm) and the elemental identification of field evaporated ions by time-of-flight mass spectrometry. The position of atoms at the sample surface is derived from the position of ion impacts on the detector.

The first prototypes (1988–1993), based on distinct detector designs, were designed at the Universities of Oxford, UK (the position sensitive atom probe, 1988) and Rouen, France (the tomographic atom probe, TAP), as well as in the USA (the optical atom probe, Oak Ridge National Laboratory) [11–13]. The French prototype (TAP, laser assisted wide angle TAP) has been commercialised by CAMECA [14]. Latter, a new generation of instrument based on the use of a local electrode (the local electrode atom probe or LEAP) was designed by Kelly and Larson at the University of Madison (USA) and commercialised by IMAGO (the first LEAP was shipped in 2001), a company founded in 1998 [15]. The latter has now joined CAMECA that is now alone on the market.

A major advantage of APT is its quantitativity combined with its high spatial resolution (0.1 nm in depth, a few nm laterally) [16,17]. The local composition in a small selected region of the analyzed volume (a few nm^3) is simply derived from the number of atoms of each species. This makes it possible the quantitative analysis of very small precipitates (a few nm in diameter) as well as the segregation of impurities to crystal defects (interfaces and grain boundaries, stacking faults, dislocations, ...).

Formerly limited to metals or good conductors, the implementation of an ultra-fast pulsed laser to the instrument (laser assisted TAP, LEAP) has opened up APT to semi-conductors and oxides and as a consequence to the important domain of microelectronics. Kellogg and Tsong were the first to implement pulsed laser beam on one-dimensional atom-probe [18]. Laser pulses give rise to very rapid thermal pulses that promote the field evaporation of surface atoms. In the instrument that we have designed in collaboration with CAMECA (FlexTAP), the specimen is field evaporated by ultrafast laser pulses (<500 fs) and the wavelength can be changed from IR to green or UV, depending on application [19–22]. This innovation has made APT a very powerful approach in nanosciences, in particular for the investigation of microelectronics materials, nanowires (silicon based or metallic) and magnetic multilayers for spintronic including tunnel junctions containing highly resistive oxide barriers [23].

Whereas the depth resolution of APT reaches the ultimate limit of a single atomic plane, the lateral resolution (parallel to the sample surface) is far from being as good. In single phase materials, the resolution reaches 0.3 nm. The atomic resolution is therefore not achieved in the three dimensions of space so that imaging the crystal lattice in 3D is generally impossible [24,25].

Unfortunately, this is not technology (detector) but physics of field evaporation that limits the lateral resolution. Aberrations in the ion trajectories very close to the tip surface are recognised to be the main source of deterioration of the spatial resolution. Atomic simulations of ion trajectories have clearly indicated that it is the subtle movements of ions leaving the surface (tip) that are responsible for the dispersion of impact positions on the detector [26,27]. These aberrations depend on the short range neighbourhood of the atom leaving the surface and on the local atomic structure and arrangement [28–30]. Ion trajectory aberrations are more pronounced close to interfaces between phases that have different evaporation fields. This leads to a more degraded spatial resolution (>1 nm) that makes tricky the measurement of the composition of nano-clusters. Several approaches have been developed to deal with this issue [31–34]. The composition of small precipitates can be measured quantitatively but systematic bias may interfere for sizes below 2–3 nm when phases have evaporation fields that differ significantly. In addition to this, field induced surface migration of atoms may also deteriorate performances [35].

3 APT sample preparation, condition of analyses and reconstructions

To produce high field ($F \sim V/R \sim$ 30–50 V/nm), APT samples are prepared in the shape of a very sharp tip with an end-radius R lower than 50 nm. The high positive voltage V (2–15 kV) that is applied promotes the field-evaporation of atoms. Contrarily to near field techniques such as scanning tunneling microscopy, the tip is the material to be analysed. But it is also important to stress out that it is the size and the shape of the tip that controls the optics of the microscope since for example the magnification is inversely proportional to the tip end radius. So, extreme care must be taken to prepare tips and information on the tip (shape, end-radius before APT experiment, ...) are primordial to understand the analysis and to further reconstruct the APT data.

Due to the final size of the tip and because the zone of interest in microelectronics sample is often/always located close to the surface, standard chemical preparations cannot be used anymore (at least for the tip preparation). Hence specific techniques have been developed to prepare tips that are all based on focused ion beam (FIB). In this work, a dual beam ZEISS NVISION40 was used to prepare the samples. For the LAWATAP and FlexTAP instruments, a first tip (iron or tungsten) must be fabricated by chemical techniques in order to reach an end-diameter of ~2 μm. Then two techniques have been developed at the GPM to place the materials to be analysed at the top of this metallic tip. The first one is a common technique originating from TEM sample preparation, the lift-out technique. Using a gallium beam, a lamella is created in the wafer and extracted using micromanipulator (Kleindik in our case). Contrarily to TEM sample preparation where the lamella is progressively thinned, the extremity of the lamella is glued on top of the previously prepared tip and

https://doi.org/10.1051/epjap/2014140060 Published online by Cambridge University Press

then cut from the lamella. Repeating this operation, 4 or 5 tips can be prepared from one extracted lamella. The second technique was developed to avoid the time consuming lift-out technique. It supposes that the starting material is a silicon wafer that is elaborated using reactive ion etching Bosch process (BP) [36] in order to create silicon posts (in our case posts of 100 μm high, 3–5 μm in diameter). Then two options are possible: (1) process the wafer (implantation, deposition, ...) after the BP, (2) use an already processed wafer and execute the BP. Both methods have been tested successfully.

Silicon posts are mechanically cut and dispersed on a glass substrate. Using a standard microscope associated with a micromanipulator, one silicon post is then glued using a conductive epoxy glue at the extremity of the metallic tip. Finally, both lift-out and posts overcome the same process, i.e., annular milling in FIB with Ga ion at 30 keV in order to obtain a tip with an end-diameter of $2R \sim 150$ nm. Finally, in order to limit the radiation damages in the final tip, the latter is imaged in FIB with Ga ions having a very low energy (2 keV). Due to difference of sputtering rate of the top of the tip (lower) as compared to the sides (higher), the end diameter of the tip decreases to the desired value. It should be noted that a protection layer is often/always deposited on the sample to protect it from Ga radiation damages. The comparison between BP and lift-out on the same sample revealed no differences in APT results. Both ways of sample preparation can be used without risks.

Once the tip is carefully prepared, it should be introduced rapidly in the APT instrument or kept under non oxidizing environment (vacuum ...). This is especially the case for silicon tips that tends to quickly oxidize once they are out of the SEM/FIB chamber. This oxide may be seen on the side of the 3D APT during the analysis and in the volume after reconstructions.

During analysis using laser-assisted APT, a crucial parameter driving the experiment is the laser wavelength and power (energy per pulse). Most of experiments were conducted using UV laser pulses that ensure good mass resolution and optimised experimental conditions for the analysis of multiphase materials containing SiO_2.

The major effect of very short laser pulses (350 fs, pulse repetition rate ∼100 kHz) that are superimposed to the steady state electric field ($F \sim V/R$ with V the applied voltage) is to lead to a sharp temperature peak that triggers field-evaporation of surface atoms. Note that the base temperature of the tip is usually set to 80 K. Experiments are always monitored so that to maintain the detection rate constant (e.g., 0.01 ion/pulse). For a tip radius almost constant (small shank angle), this means that the evaporation rate is almost constant (i.e., constant electric field for a given laser energy). Increasing the laser energy will require a lower steady-state electric field F to maintain the evaporation rate constant.

The laser power is not a very good indicator of temperature increase since the energy deposited at the tip depends on the sample and on the focalisation conditions of the laser beam, which varies from an instrument to another. A much better indicator of the electric field at the apex of the tip is the charge distribution of ions as observed in mass spectra. Indeed, it is known that surface atoms are field evaporated as singly charged ions and loose additional electrons depending on the applied field. Increasing the steady state field increases the 2+/1+ ratio as well as 3+/2+ and so forth. Hence, the charge state of silicon is a very good indicator of the static electric field. For silicon, for $Si^{++}/Si^{+} \sim 10$, the electric field is too large, leading to a high electrostatic stress leading to very frequent rapid tip fracture. When this ratio is too low, the laser power that is required to maintain constant the detection rate becomes very large. The large temperature increase may lead to many issues including surface diffusion that degrades the spatial resolution. Ablation and melting may even be observed for very large laser energy.

Figures 1a and 1b show the difference between two mass spectra of the same boron-doped silicon sample. Figures 1a and 1b correspond to a higher (resp. lower) laser power. Compared to low laser energy conditions (high field, large Si^{++}/Si^{+} ratio, Fig. 1b), complex spectrum is observed when the laser power is too high (Fig. 1a, low field, high temperature). Numerous molecular ions of silicon ($Si_2^+, Si_3^+, Si_4^+, \ldots$) are detected. The spatial distribution of boron atoms over the analysed area also show that too high laser energy are not appropriate and lead to artificial enrichment at the apex of the tip (Fig. 1c, top view [up] and side view [down]). Whereas boron atoms were homogeneously distributed in the sample associated to Figure 1b (not show here), surface migration of boron towards the apex of the tip is evidenced all along the analysis. Hence conditions of analysis and especially charge state ratio are parameter of utmost importance so that to control the field and the temperature enhancement and to avoid artefacts (artificial boron cluster at the apex, Fig. 1c).

The next step is the reconstructions of APT data. Reconstruction process requires the knowledge of the radius of curvature of the specimen all along the experiment. Several methods based on the voltage (R is proportional to V) or specimen geometry (R is proportional to depth z via the shank angle of sample as derived from SEM or TEM images) have then been developed to properly reconstruct data. In this work, reconstructions were made using specimen geometry. The reconstruction parameters were adjusted by comparing the APT volume with images or concentration profiles coming from other techniques like transmission electron microscopy (TEM) or secondary ion mass spectrometry (SIMS). Indeed, the calibration in depth using atomic planes is not possible in (1 0 0)-oriented silicon. Indeed the resolution of the laser assisted APT in depth is not sufficient to distinguish (4 0 0) planes as demonstrated in reference [21]. Some authors claimed it was possible to map out these (4 0 0) planes [37]. However, FIM (field-ion-microscopy) images of Si that we carried out (Fig. 1d) as well as APT experiments suggest that the observed "planes" are actually artefact coming from the evaporation and reconstruction processes (artificial high density layers related to evaporation bursts). FIM images

https://doi.org/10.1051/epjap/2014140060 Published online by Cambridge University Press

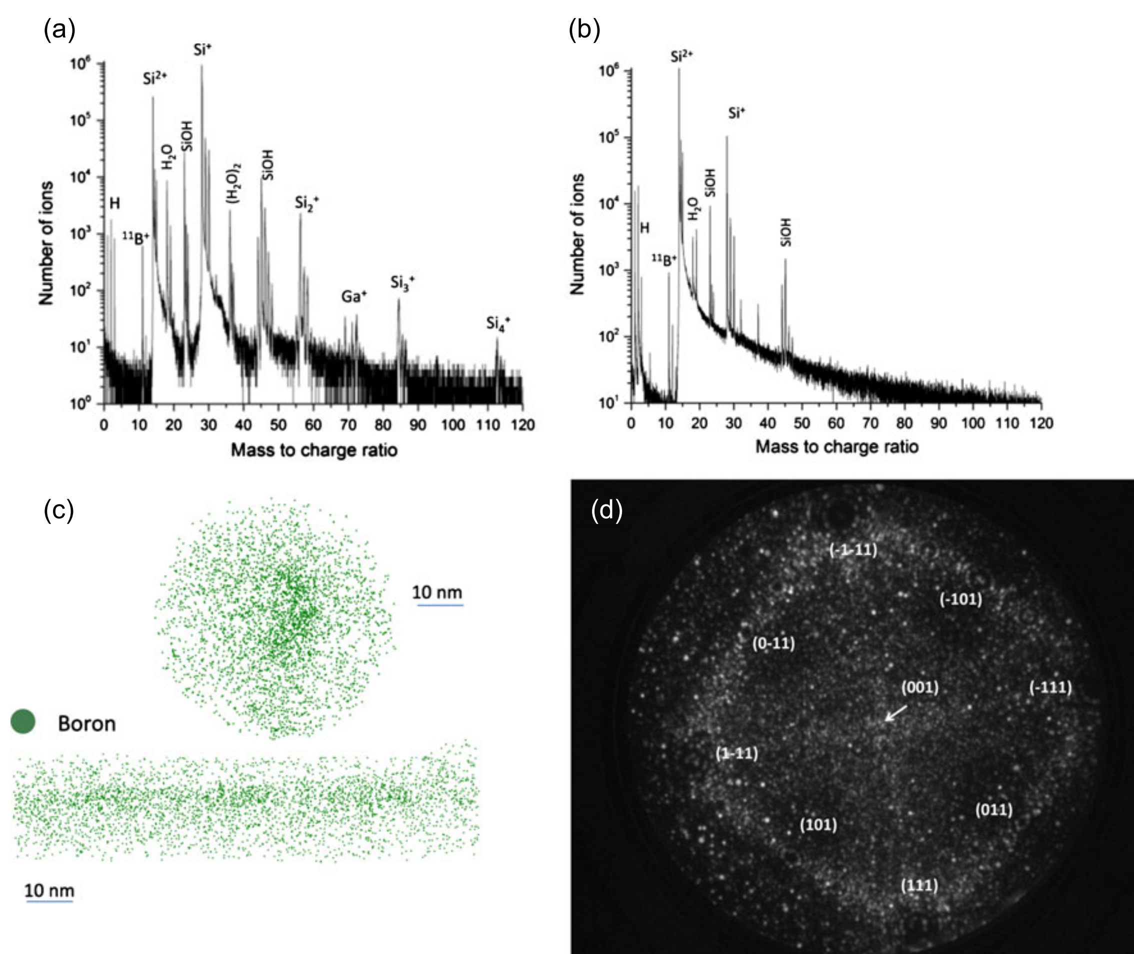

Fig. 1. (a) Mass spectrum of a boron-doped silicon sample (high laser power), (b) mass spectrum of a boron-doped silicon sample (low laser power), (c) boron distribution in a silicon sample after reconstruction in a high laser power APT analysis (top view and side view, bottom). Boron atoms tend to migrate during analysis at the apex of tip, (d) field ion microscopy (FIM) image (under H_2, $P = 2 \times 10^{-5}$ Torr, 20 K) of a (1 0 0)-oriented silicon tip. Whereas (1 1 1) and (1 1 0) poles are observed, the (1 0 0) pole cannot be imaged.

of a silicon tip made from (1 0 0)-oriented were carried out on a home-made FIM microscope (Fig. 1d) In this FIM set-up, the tip is located at 21 mm from the detector, leading to an angle of view of around 60°. This experiment was made under H_2 with a 2×10^{-5} Torr pressure at 20 K. Figure 1d demonstrates that the (1 0 0) pole cannot be resolved (center of micrograph), whereas (1 1 1), (1 1 0) and even (3 3 1) (not indicated for clarity) poles are clearly seen. This clearly suggests that (4 0 0) planes will not be resolved in APT experiments. APT analyses that we conducted indeed confirmed that (4 0 0) are not visible in reconstructions [21].

Although reconstruction procedures used in following sections were optimized, APT analyses in Sections 7 and 8 will show that a large room of improvement still exist for reconstruction procedures especially in the case of multi-phase materials like nano-transistors where local magnification effects occur. More details will be given below.

4 Distribution of Ge in SiGe epitaxial layers

SiGe epitaxial layers, that form the base of most recent bipolar transistors, were analysed using APT. The in-situ doped or Ge-enriched silicon films analysed in Sections 4–6 were grown in a 200 mm single wafer rapid thermal CVD industrial tool (HTF-Centura from Applied Materials) over monocrystalline (1 0 0) silicon wafers that undergo a high temperature prebake to ensure good epitaxial growth. The quantification of Ge in such layers is an important issue for the development of bipolar and MOS transistors as this strongly affects the layer properties and the device performance. A typical reconstruction of the volume that was analysed from a SiGe (3 at.% in Ge) epitaxial layer elaborated at 675 °C by molecular beam epitaxy is provided in Figure 2a. The Ge map clearly exhibits the presence of a sandwich structure that consists in a Ge-enriched layer comprised between two Ge-depleted layers (i.e., Si rich). Interfaces appear quite abrupt.

https://doi.org/10.1051/epjap/2014140060 Published online by Cambridge University Press

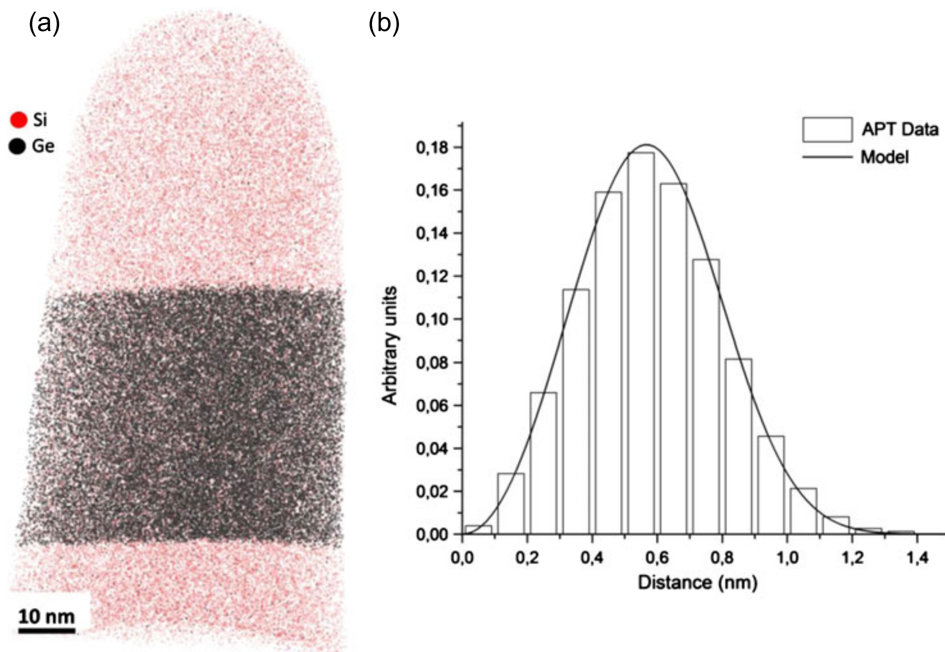

Fig. 2. (a) APT analysis of a buried SiGe layer (3 at.% in Ge), (b) frequency distribution of the distance between first neighbours for Ge atoms.

Concentration profiles (not shown here) showed that the enriched region contained around 3 at.% of Ge whereas the level of Ge in adjacent layers was close to zero (i.e., lower than the background level as revealed in mass spectrum (200 ppm, 1×10^{19} at./cm^3). The Ge map (Fig. 2a) suggests that Si and Ge atoms form a random solid solution. However this subjective observation (no Ge clustering) should be assessed using statistical tests.

The distribution of first nearest neighbour distances (1NN) between Ge atoms is an elegant approach to deal with this issue [38]. The observed distribution, the so-called 1NN distribution, is compared in Figure 2b to that expected for a random solid solution containing no Ge clusters. Theory predicts an almost symmetric distribution when no clustering occurs. Statistical tests confirm the randomness of the Si(Ge) solid solution. This is in good agreement with the Si-Ge phase diagram that exhibits an extended Si-Ge solid solution.

5 Distribution of As in epitaxial Si/Si(As)/Si layers

Arsenic doped epitaxial layers constitutes a good model of n+ emitters of nano-transistors. A high electric deactivation was measured in such epitaxial layers containing 1.5 at.% of As i.e., (7.5×10^{20} at./cm^3) elaborated at 675 °C. APT has been used to elucidate the origin of such a deactivation. The 3D map of As atoms in a Si layer sandwiched between Si layers shown in Figure 3a suggests that dopant atoms are randomly distributed. The related depth profile (Fig. 3b) indicates that the concentration of As in the Si(As) layer (7.5×10^{20} at./cm^3) is close to the expected value whereas the amount of As in the two adjacent layers is close to the APT detection limit in this experiment (5×10^{18} at./cm^3, i.e., 100 ppm). Again, the spatial distribution of As atoms in the central Si(As) layer is an important point to deal with. The 1NN distribution clearly revealed the presence of As short range ordering (clustering trend) [39]. Statistical tests confirm that Si(As) layer is not random. As tends to be surrounded by As atoms in a proportion that is larger than expected for a random solid solution. This result was confirmed on the same samples using extended X-ray absorption fine structure (EXAFS) where the probability that As atoms aggregated were first neighbours was higher than in solid solution and moreover that this probability increased with As concentration as [40]. This subtle clustering trend, evidenced by those two techniques, is thought to account for the high electrical deactivation in such highly doped layers.

When doped with 2.5 at.% of As and annealed at 675 °C, SiAs layers show a very heterogeneous distribution of As atoms (Figs. 3c and 3d) as a result of As supersaturation (the solubility limit at 675 °C is close to 1.6 at.%). This heterogeneous distribution of As Atoms is evidenced in Figure 3d (layer seen from the top). As enrichments at the nm scale appear in atomic maps (Fig. 3d). Carefull examination of reconstruction revealed the presence of self-organised As-enriched nanocolumns (ncls) 5–8 nm in diameter. It is thought that these nanocolumns have nucleated during the deposition of the epitaxial As-doped layer. 1NN tests (not shown) clearly confirmed that phase separation occur in such layers. Nano-columns (ncls) contain ∼5 at.% of As (X_β) whereas the parent phase

https://doi.org/10.1051/epjap/2014140060 Published online by Cambridge University Press

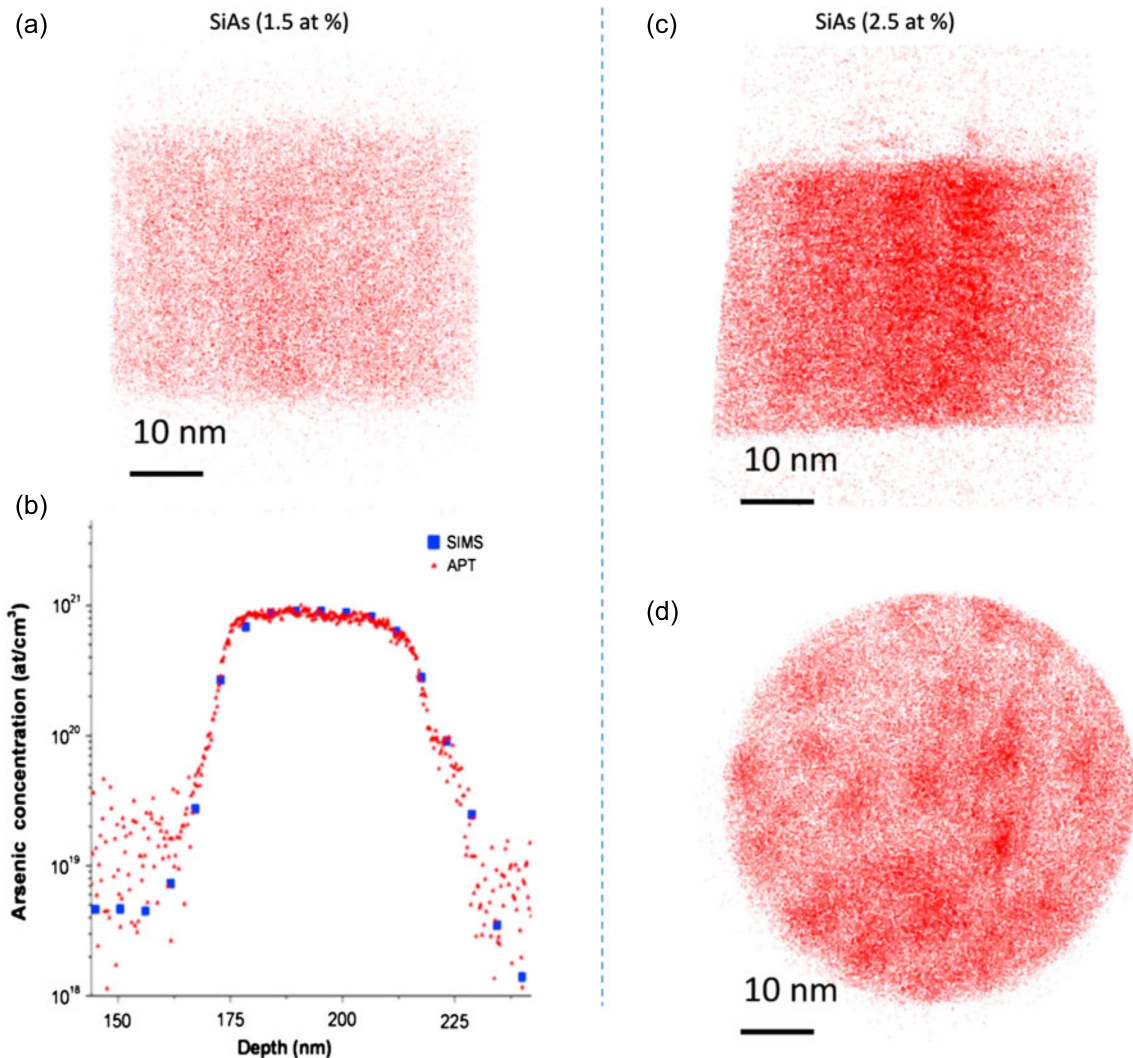

Fig. 3. (a) APT analysis of a buried SiAs layer (1.5 at.% in As), (b) concentration profile related to APT and SIMS analyses of 1.5 at.%As samples, (c) side view of an APT analysis of a buried SiAs layer (2.5 at.% in As), (d) top view of an APT analysis of a buried SiAs layer (2.5 at.% in As).

contains ∼1.5 at.% (X_α). The molar fraction f_m of second phase (ncls) as deduced from phase composition using the lever rule is close to 28.5%. The fraction of As involved in ncls as given by $f = f_\mathrm{m} \times X_\beta / X_0$, close to 57% gives an order of the atoms trapped in the nanocolumns. The As content in these ncls (5 at.%) is found much smaller than the composition of the equiatomic equilibrium phase SiAs (50 at.% of As) that is expected to precipitate in such a system. Even if trajectory overlaps cannot be ruled out, this result strongly suggests that such nanostructure is far from equilibrium. Non classical nucleation of As enriched islands is to be considered.

Similar self-organised nanostructures were observed in GeMn magnetic semiconductors thin films grown on Ge by molecular beam epitaxy (MBE) [41]. Similarly to what is observed in the present SiAs samples, Ge enriched regions were found to have a Ge content smaller that of the expected equilibrium phase. Generic kinetic Monte-Carlo simulations of unmixing during film growth (AB alloy with B content exceeding the solubility limit) that were carried out suggest that the nanostructure (mean distance between ncls and diameter) is controlled by the early stages of formation of solute enriched islands on the substrate [42]. Even if elastic interactions between ncls (misfit strains) are likely to play a role, it was found that the self-organisation is mainly controlled by diffusion length and the deposition rate.

6 Spatial distribution of As dopants in bipolar transistors

The spatial distribution of As atoms in NPN heterojunction bipolar transistors has been investigated using a dual approach combining STEM-EELS techniques and APT. Elemental EELS mapping [43] revealed a clear segregation of As to grain boundaries and the presence of a non-doped zone (NDZ) between the emitter and the Ge-enriched

https://doi.org/10.1051/epjap/2014140060 Published online by Cambridge University Press

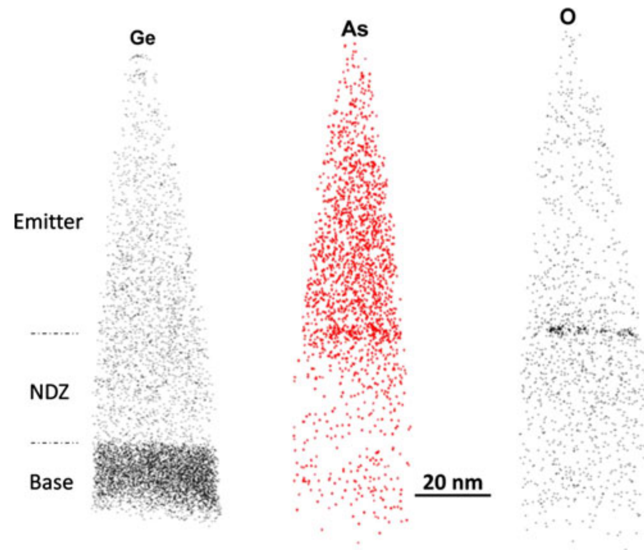

Fig. 4. 3D reconstruction of the small APT volume analysed (tip axis is vertical). Distribution of chemical species within a bipolar transistor (Ge atoms, left – As atoms, middle – O atoms, right).

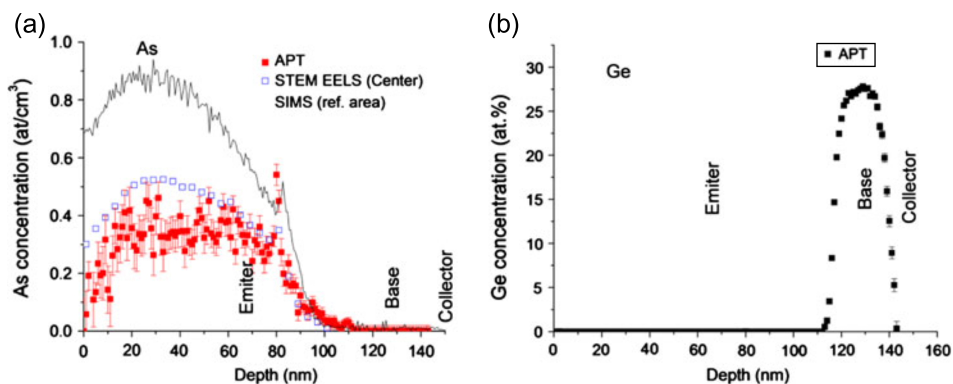

Fig. 5. (a) STEM-EELS, APT and SIMS arsenic concentration profile. Note that if STEM-EELS and APT profiles have been measured from the device, SIMS profile has been obtained from a reference area, (b) APT Ge concentration profile.

base. The NDZ was intentionally created during the process to study its influence on device performance. In the STEM image, the possibility of a very slight As enrichment was suggested at the base/NDZ interface.

A part of this transistor was thinned in the form of a sharp tip for APT analysis using FIB milling and lift-out techniques. The reconstructed volume has the shape of a truncated cone. This is due to the shank angle of the tip: the tip radius (r) increase with z (depth) leads to a decrease of the magnification ($G \sim 1/r$) that in turn leads to an increase of the analysed area ($\sim 1/G$, see reference [16] for more details). 3D reconstructions (Fig. 4) clearly exhibits three regions of the transistor namely the As-enriched emitter, the As-free NDZ as already observed by EELS, the Ge-enriched/As-depleted base. The analysis was stopped before the collector region was analysed (sample fracture under the high electric field).

This map confirms the enrichment of As at the interface between the As-enriched emitter (top of Fig. 4) and the NDZ that was previously suspected by EELS spectroscopy. However, this enrichment appears in the form of small As-enriched clusters distributed along the boundary. These tiny clusters that are present at the emitter-base interface are observed to be correlated with oxygen nanoclusters, suggesting that oxide was not completely removed during cleaning process. As atoms are thought here to diffuse and segregate to oxide clusters. These qualitative observations are confirmed in depth profiles derived from elemental maps (Fig. 5a). Arsenic enrichment above the NDZ is evident in profiles. Ge concentration reaches 25 at.% in the base region (Fig. 5b).

The comparison of APT composition profiles of As in Figure 5a (i.e., atomic fraction of As as a function of depth perpendicular to interfaces) to EELS profiles show a fairly good agreement albeit APT concentrations in the middle part of emitter appear lower than EELS measurements (0.35 at.% versus 0.5 at.%). This slight discrepancy is probably due to the fact that STEM-EELS and APT samples have not been prepared in the exact same transistor. In contrast SIMS analysis gives As levels well above

https://doi.org/10.1051/epjap/2014140060 Published online by Cambridge University Press

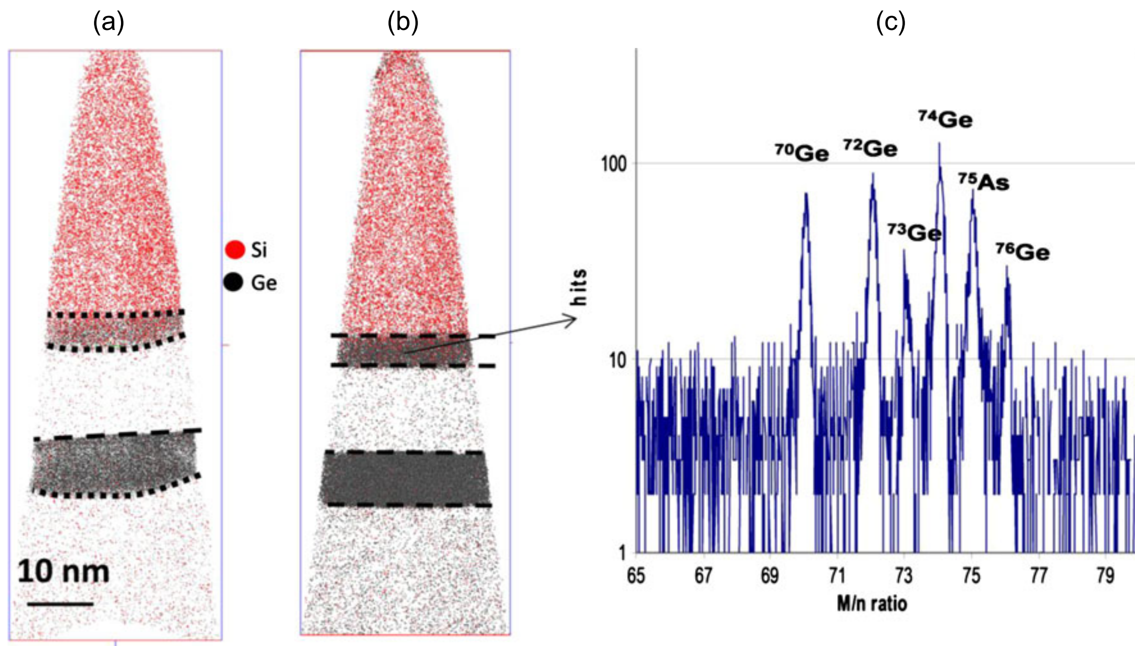

Fig. 6. (a) APT reconstruction of a bipolar transistor, (b) improved reconstruction using advanced reconstruction models [42] and (c) local mass spectrum originating from the zone evidenced in (b), demonstrating the presence of both Ge and As within the first layer.

both APT and EELS results suggesting that SIMS measurements are not representative of dopant levels in the real device (SIMS signal is integrated over a large area ($\sim 100 \times 100\ \mu m^2$) that exceeds the extent of the transistor (150 nm) and then do not account for the loss of arsenic observed by STEM-EELS on the side of the emitter region. APT reveals a greater sensitivity to the As segregation to oxygen nanoclusters as exhibited in Figure 5a, due to a higher resolution in depth.

Reconstructed layers in APT reconstructions may appear bent due to the lower evaporation field of deeper layers. This is observed in the reconstruction of Si-Ge heterojunction bipolar transistors (Fig. 6a) since Ge has a lower evaporation field compared to Si($F_{\mathrm{Si}} \sim 33$ V/nm $>$ $F_{\mathrm{Ge}} \sim 29$ V/nm). The multi-step model as developed by Vurpillot et al. was applied to rectify image distortions [44]. The resulting 3D reconstruction (Fig. 6b) shows almost flat interfaces (SiGe/Si, SiAs/Si), as observed in TEM. It is also worth mentioning that in contrast to STEM-EELS, APT is able to measure As concentration in SiGe zones. This element is clearly identified in mass spectra (Fig. 6c).

7 Distribution of dopants within a p-MOS device

The distribution of dopants within latest generations of CMOS devises (complementary metal oxide semiconductor) that are implemented in ultra-large scale integrated (ULSI) devices is of utmost importance. Observed dispersion of electrical characteristics can have dramatic effects on a technology node (Intel, 22 nm). A possible origin might originate from the redistribution of dopant atoms within the material. This may happen in various regions of MOS transistors including the gate (highly-doped polycrystalline Si) that controls the current flow in the channel, the source, that supplies charge carriers or the drain. Due to the continuous need for improvements guided by Moore's law, the doping level in these regions has continuously increased, leading to undesirable phenomena such as precipitation that is detrimental for electric activation of dopants. Even in non-supersaturated, dopants may segregate to structural defects, interfaces leading also to partial electrical deactivation.

The feasability of analysing well-established technologies such as MOS transistor [45], and more exotic structures such as FinFETs [46] or gate all aroud transistors (GAA) has been already demonstrated [47]. However, these structures nowadays contain a wide variety of materials that may have very different evaporation fields. This unfortunately leads to image distorsions in 3D resonstructions. New methods of reconstructions are currently being developed in order to take those effects into account.

Figure 7 illustrates the capability of APT to analyse and reconstruct part of a p-MOS nano-device so that to reveal the distribution of boron atoms after ion implantation in the devices. The sample was protected prior FIB milling by an amorphous Si(a-Si) cap (SEM image in Fig. 7a). In latest generation MOS transistors, the gate, that is required to have a good conductivity, is made of a heavily doped poly-crystalline silicon layer to ensure good electric conductivity. As shown in Figure 7a, an oxide was present between the amorphous Si cap and the transistor. The 3D reconstruction of a part of the transistor (Fig. 7b) is provided in Figure 8a. Again, because the

https://doi.org/10.1051/epjap/2014140060 Published online by Cambridge University Press

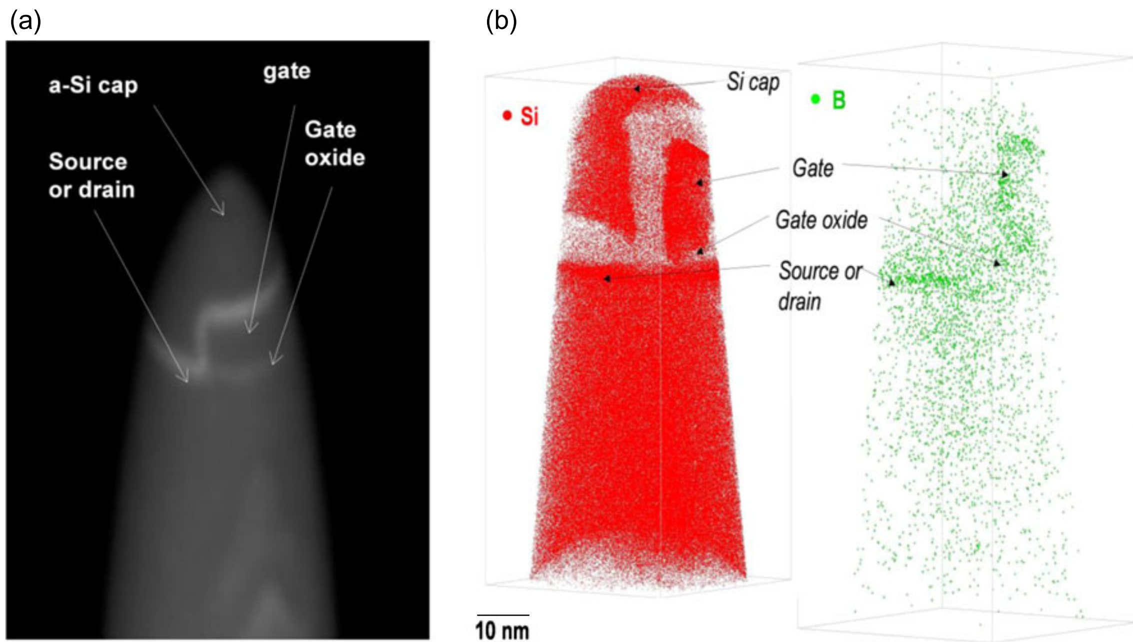

Fig. 7. (a) SEM image of the tip containing the transistor before APT analysis, (b) related APT reconstructions showing silicon and boron distributions.

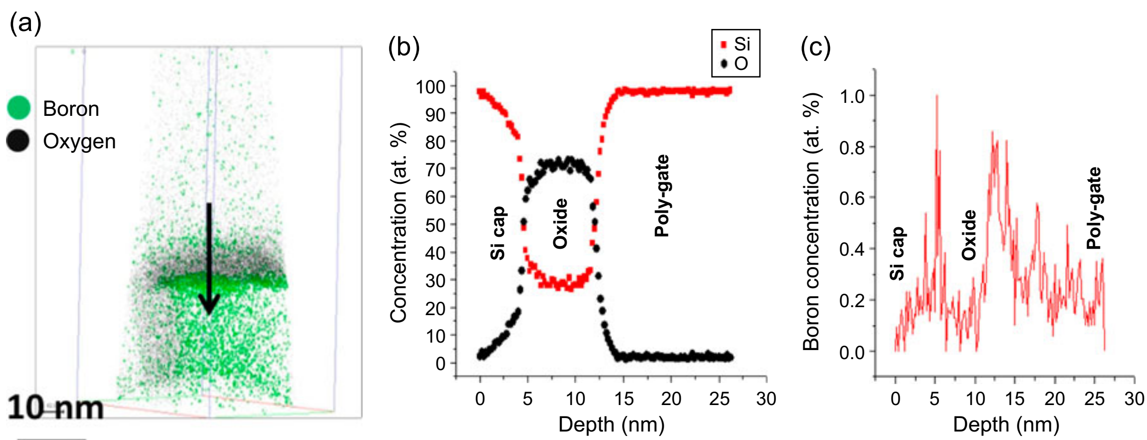

Fig. 8. (a) APT analysis of the gate of a PMOS transistor. Only oxygen atoms (black) and boron atoms (green) are represented, for clarity, (b) Si and O concentration profile through the oxide surrounding the gate, (c) associated boron concentration profile.

evaporation fields (F) of the poly-Si gate is much lower that of the surrounding SiO_2 oxide, image distortions are observed.

APT experiments also enable to focus on a selected region of the transistor (gate in Fig. 8a). The silicon oxide region (gate oxide) is clearly exhibited in the depth profile depicted in Figure 8b and identified as SiO_2 (66 at.% of O). The depth profile in Figure 8c shows that boron is subjected to large concentration fluctuations. Boron segregates to interfaces (Si-cap/oxide and oxide/poly-gate). Boron profiles suggest the occurrence of significant exo-diffusion of this element during annealing. The atomic fraction of B in the poly-Si gate is close to 0.2 at.% compared to 0.8 at.% at interfaces.

8 Three-dimensional elemental map of chemical species within gate all around devices

APT is a particularly well suited technique for the investigation of 3D architectured nano-devices like FinFET or gate all around (GAA) transistors [44]. In these devices, the gate is placed around the channel so that to better control the current flow between the source and the drain. The dopant distribution and the abruptness of interfaces are of utmost importance for performances. Electron Tomography was combined to APT to investigate such GAA devices [48]. These nano-devices are based on

https://doi.org/10.1051/epjap/2014140060 Published online by Cambridge University Press

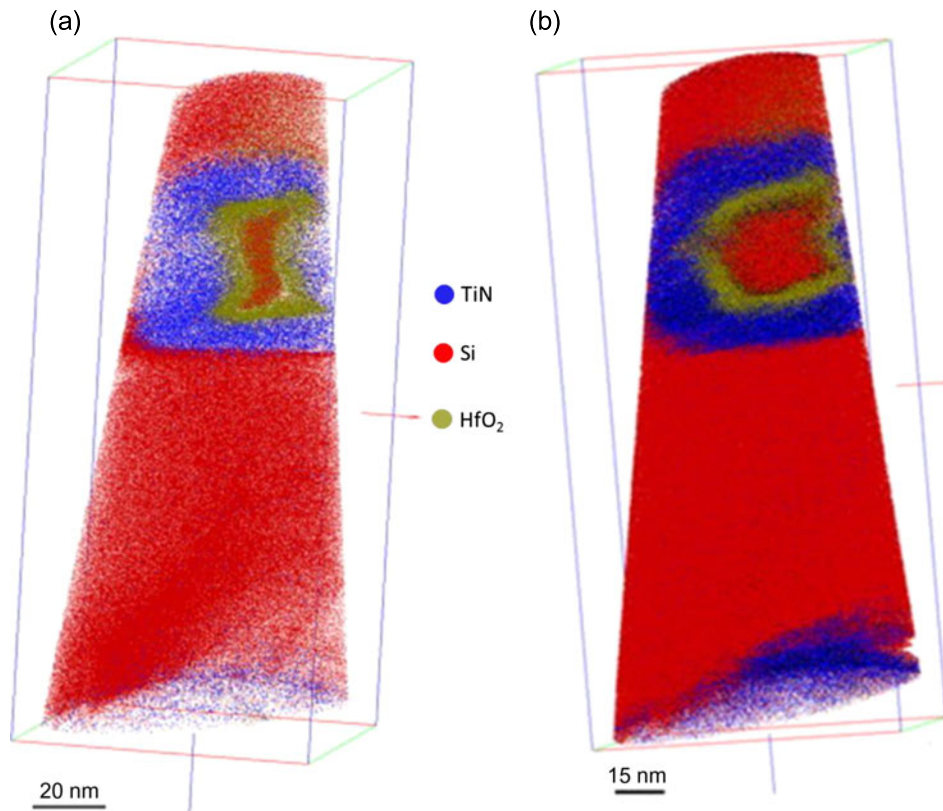

Fig. 9. 3D reconstruction of GAA transistor. The cone shape of the reconstruction is due to the shank angle of the tip analysed. The core region (i.e., Si channel, perpendicular to the tip axis) is wrapped by a SiO_2/HfO_2/TiN gate stack. (a) Original 3D reconstruction of a GAA nano-transistor, (b) corrected 3D image.

Si nanowires built from a (1 0 0) SOI substrate. The gate of such GAA nanotransistors consists in a stack of 1 nm of SiO_2, 3 nm of HfO_2 (high-k dielectric), 10 nm of TiN and 60 nm of poly-silicon (Fig. 9).

3D reconstructions revealed distorted images compared to electron microscopy that revealed square shaped channel. Strong distortions exhibited in Figure 9 are related to the high evaporation field of oxides compared to silicon (ion trajectory aberrations and local magnification effects). Reconstructions show a compression of the low field Si core (channel) that is due to focusing effects of trajectories. Ion trajectories, ion impacts and reconstructions related to a model nanostructure similar to GAA were simulated using an approach described in details elsewhere [30]. Evaporation fields of various phases were independently assessed by APT experiments conducted on SiO_2/Si, HfO_2/Si, TiN/Si samples using the evaporation field of the Si substrate as a reference (Si: 33 V/nm). The evaporation voltage thresholds of these three deposits compared to that of silicon provided the evaporation fields (SiO_2: 43 V/nm, HfO_2: 51 V/nm, TiN: 38 V/nm) that were the input data of simulations. Simulated reconstructions revealed pronounced variations of local radius in the vicinity of interfaces and were of great help for the identification of origins of image distortions [46]. Local magnification effects are known to lead to modulations of atomic density. High evaporation field oxides or TiN regions lead to protrusions at the tip surface and to defocusing effects (smaller local radius of curvature) that in turn give rise to lower impact density on the detector (i.e., low apparent atomic density in reconstructions). The apparent atomic density is thus a key experimental data that is of great help to detect and correct images [49]. A method resulting in an homogeneous distribution of the density was developed a few years ago and applied to the present data set [32]. Electron microscopy images were used to adjust dimensions in corrected APT images. Even if not perfect, corrected image (Fig. 9b) shows a geometry close to that expected. Once images corrected, APT reconstructions can be used to investigate the roughness of interfaces and the spatial distribution of chemical species in the three dimensions of space. Composition profiles through the three shells around the channel were derived. Si atoms were detected in the high-k region (HfO_2). In the present state it is however not clear whether HfO_2 really contains Si. Again, trajectory overlaps may occur and Si ions coming from SiO_2 may fall in the high-k region.

9 Conclusion

The implementation of ultra-fast laser pulses to APT (instead of HV pulses) has been a major breakthrough in the story of atom probe tomography. This has extended

https://doi.org/10.1051/epjap/2014140060 Published online by Cambridge University Press

its application field to bad conductors and consequently to microelectronics. Impressive results were recently published [43]. Recent papers give more details on experimental conditions and potential of this new generation of atom-probe in nanosciences [50–53].

Compared to SIMS, a key tool in microelectronics, APT has many advantages (3D imaging, spatial resolution) but it has also several shortcomings or drawbacks (preparation of specimen, fracture of tips under the high electrostatic stress applied [limited life time of specimens], mass resolution, statistics and sensitivity). Instruments are in fact more complementary than concurrent. Statistical fluctuations in APT are larger because of the smaller volume analysed compared to SIMS. The analysed area of SIMS (100 μm wide except in Nano-SIMS), 10^6 times larger than that of APT (100 nm wide) combined with its higher mass resolution (less noise in the narrower selection mass window) leads to much better sensitivity (1 appm versus 10–100 ppm for APT). Even if the low ionization efficiency of SIMS (between 0.1% and 1%) compared to APT (ionization rate = 1, detection efficiency $Q = 0.5$) reduces the difference of collected ions (N), statistics remain much better in SIMS analysis (a factor close to 30). However, this advantage is counterbalanced by the higher lateral resolution of APT and its unique 3D imaging capability.

APT reconstructions of complex architectures composed of materials with different evaporation fields are subjected to distorsions caused by trajectory aberrations. This is a key problem that originates from the early step of field evaporation of surface atoms. Atomistic simulations were shown to be of great help to assess distortions and their origin as well as to correct images. However, this issue remains a complex and open question with no general answer.

Recent developments in transmission electron microscopy during the last decade have been very impressive and demonstrate that electron tomography at a comparable scale is now available. Material containing finely dispersed precipitates a few nm in size can for instance be imaged in 3D using both techniques. Such a correlative approach can be of great help to asses APT image distortions and correct images. Comparison between reconstructed volumes was recently achieved [54]. However the atomic-scale is not yet achievable in electron tomography and quantitative data on the composition of nanoobjects appear to be less evident or straightforward than with APT.

Electron energy loss spectroscopy, energy filtering as well as energy dispersive techniques are alternative nanoanalysis techniques that can be combined with APT in a very fruitful way (correlative microscopy and analysis). The “atom-scope project” precisely aims to combine TEM and APT in a single instrument [55].

Research on semiconductors were supported by ANR fundings (Project no. APTITUDE ANR-12-NANO-0001). The authors greatly acknowledge STMicroelectronics to supply samples, and in particular Pierre Morin for MOS transistors, Germain Servanton and Roland Pantel for bipolar transistors and epitaxial layers, CEA-LETI for very fruitful scientific collaborations, F. Vurpillot for his help in APT reconstructions, G. Da Costa for help in FIM analyses, M. Raghuwanshi for experiments on boron doped silicon samples with high lasesr power and E. Cadel for sample preparation.

References

1. S. Duguay, A. Colin, D. Mathiot, P. Morin, D. Blavette, J. Appl. Phys. **108**, 034911 (2010)
2. O. Cojocaru-Mirédin, D. Mangelinck, K. Hoummada, E. Cadel, D. Blavette, Scripta Mater. **57**, 373 (2007)
3. O. Cojocaru-Mirédin, C. Perrin-Pellegrino, D. Mangelinck, D. Blavette, J. Appl. Phys. **108**, 033501 (2010)
4. O. Cojocaru-Mirédin, D. Mangelinck, D. Blavette, J. Appl. Phys. **106**, 113525 (2009)
5. D. Blavette, H. Wang, M. Bonvalet, F. Hüe, S. Duguay, Phys. Status Solidi A **211**, 126 (2013)
6. K. Thompson, P.L. Flaitz, P. Ronsheim, D.J. Larson, T.F. Kelly, Science **317**, 1370 (2007)
7. K. Inoue, F. Yano, A. Nishida, T. Tsunomura, T. Toyama, Y. Nagai, M. Hasegawa, Appl. Phys. Lett. **93**, 133507 (2008)
8. K. Inoue, F. Yano, A. Nishida, H. Takamizawa, T. Tsunomura, Y. Nagai, M. Hasegawa, Appl. Phys. Lett. **95**, 043502 (2009)
9. D.J. Larson, A. Cerezo, J. Juraszek, K. Hono, G. Schmitz, MRS Bull. **34**, 732 (2009)
10. E.W. Müller, J. Panitz, S.B. Mc Lane, Rev. Sci. Instrum. **39**, 83 (1968)
11. A. Cerezo, I.J. Godfrey, G.D.W. Smith, Rev. Sci. Instrum. **59**, 862 (1988)
12. A. Bostel, D. Blavette, A. Menand, J.M. Sarrau, J. de Phys. **C8-50**, 501 (1989)
13. M.K. Miller, Surf. Sci. **266**, 494 (1992)
14. D. Blavette, A. Bostel, J.M. Sarrau, B. Deconihout, A. Menand, Nature **363**, 432 (1993)
15. T.F. Kelly, D.J. Larson, Mater. Charact. **44**, 59 (2000)
16. F. Vurpillot, G. Da Costa, A. Menand, D. Blavette, J. Microsc. **203**, 295 (2001)
17. B. Gault, M. Moody, F. De Geuser, A. La Fontaine, L.T. Stephenson, D. Haley, S.P. Ringer, Microsc. Microanal. **16**, 99 (2010)
18. G. Kellogg, T.T. Tsong, J. Appl. Phys. **51**, 1184 (1980)
19. B. Gault, A. Vella, F. Vurpillot, A. Menand, D. Blavette, B. Deconihout, Ultramicroscopy **107**, 713 (2007)
20. B. Deconihout, F. Vurpillot, B. Gault, G. Da Costa, M. Bouet, A. Bostel, D. Blavette, A. Hideur, G. Martel, M. Brunel, Surf. Interface Anal. **39**, 278 (2007)
21. E. Cadel, F. Vurpillot, R. Larde, S. Duguay, B. Deconihout, J. Appl. Phys. **106**, 044908 (2009)
22. B. Gault, F. Vurpillot, A. Vella, M. Gilbert, A. Menand, D. Blavette, Rev. Sci. Instrum. **77**, 043705 (2006)
23. D. Blavette, T. Al Kassab, E. Cadel, A. Mackel, M. Gilbert, O. Cojocaru, B. Deconihout, Int. J. Mat. Res. **99**, 454 (2008)
24. F. Vurpillot, L. Renaud, D. Blavette, Ultramicroscopy **95**, 223 (2003)

https://doi.org/10.1051/epjap/2014140060 Published online by Cambridge University Press

25. M.P. Moody, B. Gault, L.T. Stephenson, D. Haley, S.P. Ringer, Ultramicroscopy **109**, 815 (2009)
26. F. Vurpillot, A. Bostel, A. Menand, D. Blavette, Eur. Phys. J. Appl. Phys. **6**, 217 (1999)
27. F. Vurpillot, A. Bostel, D. Blavette, J. Microsc. **196**, 332 (1999)
28. A.R. Waugh, E.D. Boyes, M.J. Southon, Surf. Sci. **61**, 109 (1976)
29. F. Vurpillot, A. Bostel, E. Cadel, D. Blavette, Ultramicroscopy **84**, 213 (2000)
30. F. Vurpillot, A. Bostel, D. Blavette, Appl. Phys. Lett. **76**, 3127 (2000)
31. F. Vurpillot, A. Cerezo, D. Blavette, D.J. Larson, Microsc. Microanal. **10**, 384 (2004)
32. F. De Geuser, W. Lefebvre, F. Danoix, F. Vurpillot, B. Forbord, D. Blavette, Surf. Interface Anal. **39**, 268 (2007)
33. T. Philippe, M. Gruber, F. Vurpillot, D. Blavette, Microsc. Microanal. **16**, 643 (2010)
34. C. Oberdorfer, G. Schmitz, Microsc. Microanal. **17**, 15 (2011)
35. B. Gault, M. Muller, A. La Fontaine, M.P. Moody, A. Shariq, A. Cerezo, G.D.W. Smith, J. Appl. Phys. **108**, 044904 (2010)
36. D.J. Larson, R.L. Martens, T.F. Kelly, M.K. Miller, J. Appl. Phys. **87**, 5989 (2000)
37. K. Hoummada, D. Mangelinck, B. Gault, M. Cabié, Scripta Mater. **64**, 378 (2011)
38. T. Philippe, S. Duguay, G. Grancher, D. Blavette, Ultramicroscopy **132**, 114 (2013)
39. S. Duguay, F. Vurpillot, T. Philippe, E. Cadel, R. Larde, B. Deconihout, G. Servanton, R. Pantel, J. Appl. Phys. **106**, 106102 (2009)
40. G. Servanton, Ph.D. thesis, Université Joseph Fournier, Grenoble, France, 2010
41. I. Mouton, R. Lardé, E. Talbot, E. Cadel, C. Genevois, D. Blavette, V. Baltz, E. Prestat, P. Bayle-Guillemaud, A. Barski, M. Jamet, J. Appl. Phys. **112**, 113918 (2012)
42. I. Mouton, R. Larde, E. Talbot, C. Pareige, D. Blavette, J. Appl. Phys. **115**, 053515 (2014)
43. A. Claverie, *Transmission Electron Microscopy in Micro-nanoelectronics* (Wiley Publication, Chichester, 2012), pp. 50–51
44. F. Vurpillot, M. Gruber, G. Da Costa, I. Martin, L. Renaud, A. Bostel, Ultramicroscopy **111**, 1286 (2011)
45. K. Inoue, F. Yano, A. Nishioda, H. Takamizawa, Y. Nagai, M. Hasegawa, Ultramicroscopy **109**, 1479 (2009)
46. M. Gilbert, W. Vandervorst, S. Koelling, A.K. Kambham, Ultramicroscopy **111**, 530 (2011)
47. A. Grenier, D. Cooper, K. Tachi, T. Ernst, S. Duguay, E. Cadel, F. Bertin, A. Chabli, in *Proceedings of ICM17, Rio de Janeiro (Brazil) 2010*
48. A. Grenier, S. Duguay, J.P. Barnes, R. Serra, G. Haberfehlner, D. Cooper, F. Bertin, S. Barraud, G. Audoit, L. Arnoldi, E. Cadel, A. Chabli, F. Vurpillot, Ultramicroscopy **136**, 185 (2014)
49. D. Blavette, F. Vurpillot, P. Pareige, A. Menand, Ultramicroscopy **89**, 145 (2001)
50. G. Sha, S.P. Ringer, Ultramicroscopy **109**, 580 (2009)
51. K.L. Torres, G.B. Thompson, Ultramicroscopy **109**, 606 (2009)
52. M. Gruber, C. Oberdorfer, P. Stender, G. Shmitz, Ultramicroscopy **109**, 654 (2009)
53. A. Nishimura, K. Nogiwa, T. Otobe, T. Okhubo, K. Hono, K. Kondo, A. Yokoyama, Ultramicroscopy **109**, 467 (2009)
54. I. Arslan, E.A. Marquis, M. Homer, Ultramicroscopy **108**, 1579 (2008)
55. M.K. Miller, T.F. Kelly, in *Proceedings of ICM17, Rio de Janeiro (Brazil), 2010*

https://doi.org/10.1051/epjap/2014140060 Published online by Cambridge University Press